32-GHz Performance of the DSS-14 70-Meter Antenna: 1989 Configuration

M. S. Gatti
Ground Antenna Facilities and Engineering Section

M. J. Klein and T. B. H. Kuiper
Space Physics and Astrophysics Section

The results of preliminary 32-GHz calibrations of the 70-meter antenna at Goldstone are presented. Measurements were done between March and July 1989 using Virgo A and Venus as the primary efficiency calibrators. The flux densities of these radio sources at 32 GHz are not known with high accuracy, but were extrapolated from calibrated data at lower frequencies. The measured value of efficiency (0.35) agreed closely with the predicted value (0.32), and the results are very repeatable. Flux densities of secondary sources used in the observations were subsequently derived. These measurements were performed using a beamswitching radiometer that employed an uncooled high-electron mobility transistor (HEMT) low-noise amplifier. This system was installed primarily to determine the performance of the antenna in its 1989 configuration, but the experience will also aid in successful future calibration of the Deep Space Network (DSN) antennas at this frequency.

I. Introduction

NASA/JPL is planning to use the 32-GHz frequency band for communications and navigation of future deep-space missions. Performance estimates of existing and future ground station capabilities are needed for both mission planning and technology development. A research and development radiometer has been placed on the DSS-14 70-meter antenna as a precursor to the implementation of 32-GHz systems on the 70-meter antenna network. The radiometer will be used to determine the current performance characteristics of the large antennas at this frequency and to determine what upgrades may be advisable for future systems. Our experience with the 70-meter calibrations will also contribute to successful calibrations of the new 34-meter antennas, which will be built in the future.

This article describes the measurements performed at 32 GHz between March and July, 1989, on the recently upgraded (64-m) 70-meter antenna at Goldstone (DSS-14). These measurements were done on seven separate days by using radiometric observations of six astronomical radio sources: 3C274 (Virgo A), 3C273, 3C84, 3C286, $P2134+004$, and Venus.

It is important to note that the flux densities of natural radio sources are not accurately known at 32 GHz. Very few attempts to calibrate radio source intensities on an absolute scale have been reported above 10 GHz, so that microwave spectra of even the most intense radio sources are increasingly uncertain at high frequencies. Estimates of the uncertainty in the absolute flux density scale at 32 GHz are typically 10 percent or more. The precision of the measurements reported in this article is sufficiently high that error estimates for the results are clearly dominated by the absolute flux error and not by random errors.

II. Radiometer Description

A. Description

At 32 GHz, radiometry is complicated by tropospheric effects. Specifically, the system operating temperature varies due to clouds, moisture, and other weather phenomena. The measurement accuracy of the increase in system temperature due to a radio source is, therefore, significantly impacted for all but the best of observing conditions. There are techniques to eliminate these adverse effects; the most common one is to use a beam-switching radiometer. This radiometer is an adaptation of the one proposed by Dicke [1] wherein the difference in temperature between a reference signal and the unknown signal is measured by the system. For our radiometer, the reference signal is derived from an antenna beam pointing slightly off-axis of the desired antenna beam. The reference is the cold sky, and the unknown is the source temperature plus the cold sky. The difference in detected power is, therefore, proportional to the source temperature.

The reference signal is detected when the system is switched to the second feedhorn, which is laterally displaced from the Cassegrain focus of the 70-meter reflector. For this application, the displacement is 3.375 inches. This displacement produces a beam for this feed that is offset approximately 30 millidegrees lower in elevation than the beam produced by the on-axis feed (boresight) of the antenna. This represents approximately 4 beamwidths of the pattern defined by the on-axis feed. This technique is similar to that proposed by Slobin, et al. [2]. The off-axis reference antenna beam is used to provide an "off-source" reference temperature for the Dicke switched radiometer. For this purpose, the reference beam need not be precisely matched to the on-axis beam, but the cancellation of variations in sky emission is improved if the two beams yield nearly identical system temperatures when each in turn is directed at the sky.

Figure 1 shows a block diagram of the radiometer system. Figure 2 is a photograph of the system as assembled for test. The block diagram shows the two separate feedhorns, each of which produces an antenna beam when placed on the 70-meter antenna. The feedhorn that produces beam 1 (as designated on the block diagram) is placed at the focal point of the reflector system. The signals from each beam are alternately sampled by a circulator switch that operates between 2 and 20 Hz. The low-noise amplifier (LNA) consists of a high-electron mobility transistor (HEMT) device. The system requires no cryogenic devices and is quite compact. The remaining portions of the system consist of follow-up amplifiers, downconverters, detectors, and a Stanford Research SR-510 lock-in amplifier.

The signal from the Dicke switch is a modulated square wave that is the difference between the signals in the two beams. The lock-in amplifier demodulates this signal and produces the desired difference signal. The strip chart recorder plots this difference signal as a function of time. If each antenna beam is observing the same target, such as the sky, and if the system is perfectly balanced, a zero signal from the lock-in amplifier is recorded. When beam 1 is pointed to a radio source and beam 2 is off the source, the signal is proportional to the increase in system temperature due to the radio source. The output from a diode noise source is coupled into the waveguide of beam 1 to calibrate the system. The diode calibration is routinely switched on several times each hour as the radio sources are observed. With this procedure, the increase in system temperature produced by each radio source is calibrated, and the adverse effects of gain variations in the HEMT and receiver are virtually eliminated. The aperture efficiency of the antenna is then derived from the measured source temperatures and the assumed values of the source flux densities at 32 GHz (see Section IV).

The radiometer was placed in the XKR feedcone of the 70-meter antenna at Goldstone. This feedcone contains other hardware, including a 22-GHz Dicke beamswitching radiometer and the X-band planetary radar. Figure 3 shows the top of this feedcone, including the variety of feeds. The front-end portion of the radiometer, consisting of the feeds, waveguides, switches, amplifiers, and downconverter, is located with the feeds in the feedcone. The intermediate frequency (IF) signal is sent via coaxial cable from the feedcone to the pedestal room where the lock-in amplifier, square-law detector, recorder, and pulse generator are located.

B. Operating Characteristics

The operating characteristics of the radiometer are defined by several quantities, the most important of which are

the stability and the operating system temperature, T_{op}. These characteristics limit the sensitivity of the system and determine the configuration of the actual observations, i.e., switching rates, bandwidths, follow-up amplifier gain, etc. The individual components for this system were measured and their contributions to T_{op} were determined. Table 1 shows the individual contributions to the system temperature (see Section III for definitions). Also, the system temperature was measured by the calibration techniques discussed in the next section. The measured value and predicted value of T_{op} agreed remarkably well. For these and all subsequent measurements, the reference plane for T_{op} was at the input to the feedhorn (due to the calibration technique). The tolerances reported in this article have 2σ (95 percent) confidence. The final result is that the effective receiver temperature T_e equals 391 (± 8) kelvin. When the effects of the atmosphere and galactic background are included (by estimates), it is expected that T_{op} will be 410 (± 10) kelvin. Actual measurements at DSS-14 indicate a T_{op} of 415 (± 7) kelvin. The next section provides the details of the calculation and calibration.

The radiometer settings for our observations are given in Table 2. Included in this table are the time constants for the power integration, switching rates for the Dicke switch, IF bandwidth, and HEMT gain.

III. Calibration Techniques

A. Definitions

In this section, the quantities used in the calculation of the system temperatures and the quantities used to calibrate the system are defined. Following sections show the equations used to perform the calibration and calculations. The definitions (all temperatures in kelvin) are as follows:

T_{op} = operating system temperature of radiometer

T_a = effective antenna temperature

T_e = effective receiver temperature

T_{sky} = total temperature due to the sky contribution

T_{atm} = temperature due to the atmosphere

T_{gal} = 3.0-K cosmic background radio emission

T_{so} = temperature contribution due to feed spillover

T_{qs} = temperature contribution due to quadrupod scattering

T_{tl} = temperature due to the transmission line between amplifiers and feed (including switches)

T_p = physical temperature of transmission line (300 K)

T_m = temperature due to the LNA

T_{etc} = temperature due to the follow-up equipment, including the downconverter and IF equipment

T_f = temperature of T_{etc} referenced to the input of the LNA, called "follow-up" temperature

G_{tl} = gain of the transmission line (< 1)

L_{tl} = loss of the transmission line $= 1/G_{tl}$

G_m = gain of the LNA

For any measurement, the reference plane location for calibration must be explicitly stated since the resulting temperatures depend on reference location. In the calibrations performed, the measurement reference plane was located at the aperture of the feedhorn. Therefore, this position was chosen for reporting the various temperatures and noise diode values.

B. Calculation of System Parameters

For the reference plane chosen in this work, the calculation of T_{op} was performed using the following equations:

$$T_{op} = T_a + T_e \tag{1}$$

$$T_a = T_{sky} + T_{so} + T_{qs} \tag{2}$$

$$T_{sky} = T_{atm} + T_{gal} \tag{3}$$

$$T_e = T_l + \frac{T_m}{G_{tl}} + \frac{T_{etc}}{G_{tl}G_m} \tag{4}$$

$$T_l = (L_{tl} - 1)T_p \tag{5}$$

$$T_f = \frac{T_{etc}}{G_m} \tag{6}$$

Combining Eqs. (2) through (6) into Eq. (1) yields

$$T_{op} = \left[(T_{atm} + T_{gal} + T_{so} + T_{gs})\right] + \left[(L_{tl} - 1)T_p + L_{tl}(T_m + T_f)\right] \tag{7}$$

Using Eq. (7) and the information in Table 1, the value of T_{op} is expected to be 409.5 K, which may be compared to the measured value given earlier as 415 K.

C. Aperture Load and Noise Diode Calibrations

The calibrations to determine the system temperature, sky temperature, effective receiver temperature, and noise diode temperature were performed using an aperture loading technique [3]. This technique uses one microwave absorber (a blackbody source) at ambient temperature, $\approx$ 300 K, and another that is also soaked in a bath of liquid nitrogen, temperature $\approx$ 77 K. The two absorbers were placed in turn over the aperture of the feed for successive measurements of power. This was done by carrying the absorber, a styrofoam container, and liquid nitrogen to the feedcone and manually holding the absorber over the aperture. Noise power measurements were made on each aperture load with the noise diode turned on and off. A power meter was used to measure the IF signal in total power mode, i.e., the radiometer was not Dicke switching. The measurement was done repeatedly for approximately 5 minutes in order to minimize the time that the absorber was in the nitrogen bath for the cold load case. In this way, the effects of ice crystallization in the styrofoam and absorber were reduced. The actual temperature of the ambient load is measured by a thermometer, whereas the cold load was assumed to be 77 K. Typically, eight to ten measurements of the quantities defined below were obtained in the 5 minute period. Before calculating the quantities of interest, the following symbols are defined:

Let

$$Y_1 = \frac{P_h}{P_{sky}} = \frac{\text{Power looking at hot load}}{\text{Power looking at sky}} \tag{8}$$

$$Y_2 = \frac{P_c}{P_{sky}} = \frac{\text{Power looking at cold load}}{\text{Power looking at sky}} \tag{9}$$

$$Y_3 = \frac{P_h}{P_c} = \frac{\text{Power looking at hot load}}{\text{Power looking at cold load}} \tag{10}$$

$$Y_4 = \frac{P_{sky/nd}}{P_{sky}} = \frac{\text{Power looking at sky noise diode on}}{\text{Power looking at sky}} \tag{11}$$

From Eqs. (8) through (11) it can be shown that the following parameters result:

$$T_{op} = \frac{T_h - T_c}{Y_1 - Y_2} \tag{12}$$

$$T_e = \frac{T_h - Y_3 T_c}{Y_3 - 1} \tag{13}$$

$$T_{nd} = T_{op}(Y_4 - 1) \tag{14}$$

$$T_a = T_{op} - T_e \tag{15}$$

where T_h is the temperature of the hot load, T_c is the temperature of the cold load, and T_{nd} is the noise diode temperature at the measurement reference plane. The measured values for these parameters are found in Table 3.

A total of 31 noise diode calibrations were done on three separate days during this observation period. Using Eqs. (12) through (15), it was determined that the noise diode was quite steady regardless of the outside temperature conditions, probably because the XKR feedcone is temperature controlled. The outside temperature varied from 14.5 degrees C to 31 degrees C, while the cone temperature range was only 18.5 degrees C to 22 degrees C. This is mentioned because the noise diode for this experiment was not in an environmentally controlled box or oven that would improve the stability of the noise diode signal. Table 3 shows the normal standard deviation of the 31 measurements for each of the given quantities.

From Tables 1 and 3 it can be seen that there is excellent agreement between the measured value of T_{op} (Table 3) and the predicted value (Table 1). Also, there is excellent agreement between the measured value of T_e (Table 3) and the predicted value (Table 1). The temperature contribution due to the atmosphere is often important. For each of our calibrations, the weather was clear and calm with low humidity. From Eq. (15) T_a can be calculated, which from Eq. (2) allows estimates of T_{atm}. If T_{gal} is assumed to be 3 K, the quadrupod and spillover are assumed to be 6.5 K [4]. Thus, T_{atm} can be estimated to be 6.6 K.

The linearity measurement of the system is a by-product of the noise diode and system temperature calibrations. By injecting the noise diode into the signal path during the hot load, cold load, and sky measurements, the effects of errors due to system linearity may be calculated. This is done by comparing the noise diode value calculated from Eq. (14) using different Y_4 factors; specifically, by using observations made looking at the hot and cold load with and without the noise diode, as is done when observing the sky. Observations indicated the difference in measured noise diode values is small enough to indicate a linear system. It is usually thought that if the linearity error is small, no correction should be performed since the correction is frequently based on a model that may have errors of the same order of magnitude as the linearity error itself.

IV. Radio Source Data

A. Radio Sources

Several criteria were used to select appropriate radio sources for the antenna performance measurements. First, it was very important to observe the radio galaxy Virgo A (3C274) so that the antenna gain measurements could be traced to the Virgo A microwave spectrum, which is consistently referenced in the radio astronomy literature. It is one of the few sources whose spectrum has been calibrated over a wide range of the microwave frequencies (e.g., see Baars et al. [5]). Although the solid angle of the Virgo A source is not especially small compared to the half-power beamwidth of the 70-m antenna operating at 32 GHz, it is by far the most compact of the sources that have been used to calibrate the absolute scale of the microwave flux density spectrum.

A second source selected for gain calibration purposes was Venus, which is an intense radio source at short centimeter wavelengths. The planet's dense atmosphere exhibits a thermal emission spectrum with an equivalent black body temperature of 475 K at 32 GHz [6]. The planet was located near the far side of its orbit during the observations, and this fortuitous location meant that the angular diameter was near its minimum value and much smaller than the antenna beam. Venus also has an advantage in that models of the radio emission spectrum have been computed by applying radiative transfer theory to the physical and chemical properties of the planet's atmosphere. The properties of the atmosphere on a global scale are quite well-known from the in situ data returned by U.S. and Soviet probes and orbiting spacecraft. In addition, years of ground-based astronomical studies have added other critical information to the theoretical work.

Four other sources were included. The variable radio sources 3C84 and 3C273 were observed because they are intense emitters at 32 GHz and they have very small angular diameters (< 0.0005 degrees ≈ 1.8 arcseconds), which makes them very useful for measuring the antenna beam parameters. Both are known to be variable on timescales of weeks or months, so they can only be used for relative antenna gain measurements. The sources 3C286 and P2134+004 also were observed as a consistency check to see if the new flux density results agreed with extrapolations of their published spectra to 32 GHz.

Several other sources that would have been useful are not included in this article. Some were simply not available during the time scheduled for the experiments, and others were eliminated because of time constraints. One of these was the planet Mars, which was not favorably positioned at the time. Two others were DR21 and NCG7027, whose flux densities are thought to be known within reasonable tolerances. In fact, DR21 was observed, but the measurements appeared to be contaminated by one or more nearby sources. DR21 lies in a highly complex region of thermal emission sources in the plane of the galaxy, and the presumption is that the angular separation of the two antenna beams is small enough that the reference antenna beam is detecting neighboring sources of emission. Additional work on this problem is planned.

Table 4 lists the six sources that were used in the calibration and summarizes the measured flux density, S; the associated increase in antenna temperature at the reflector-set angle of 45 degrees, T_s, of the four secondary sources; the source size correction factors, C_r; and the increase in antenna temperature for a 100 percent efficient antenna. This increase in antenna temperature is given by:

$$T_{100} = \frac{SA_p}{2kC_r} \tag{16}$$

where k is the Boltzmann constant, $k = 1.38062 \times 10^{-23} Ws^{-1}K^{-1}$; and A_p is the physical aperture size of the antenna, $A_p = \frac{\pi D^2}{4}$. The efficiency is thus given by

$$\eta = \frac{T_s}{T_{100}} \tag{17}$$

B. Flux Densities

The flux densities for Virgo A and Venus were used for the aperture efficiency measurements. From the microwave spectrum of Virgo A published by Baars et al. [5], the flux density at 32 GHz should be $14.68 J_y \pm 0.8 J_y$ (1σ), where 1 J_y = 1 Jansky = 10^{-26} Wm^{-2} Hz^{-1}. The uncertainty is larger than those usually quoted at longer wavelengths because the spectrum (thought to be linear) must be extrapolated to 32 GHz from 25 GHz, which marks the upper-frequency limit of the absolute measurements that have been published for this source.

The flux density, S, for Venus is calculated from the disk-averaged brightness temperature and the solid angle of the planet. The expression for the flux density, using the Rayleigh-Jeans approximation to the blackbody radiation equation, is

$$S = \frac{(2kT)\Omega}{\lambda^2} \tag{18}$$

where $\lambda = 0.009375$ m is the wavelength of the observations, and $T = 475 \pm 25$ K (1σ) is the brightness tempera-

ture of Venus at 32 GHz [6]. The solid angle of the planet, $\Omega = \pi r^2/d^2$, was calculated with the known distance, d, of Venus for each observation. The effective radius, r, of the thermally emitting atmosphere of Venus is 6120 km [7]. Table 4 shows the flux density of Venus for the two separate days it was observed.

C. Radio Source Size Correction Factors

It is an unfortunate fact that radio sources bright enough for microwave calibration purposes are either time variable or they are partially resolved by the compact beamwidths of modern antennas operating at short centimeter wavelengths. It is possible to correct for the partial resolution of sources if their angular dimensions are smaller than the antenna beamwidth. Only two of the observed sources, Venus and Virgo A, have angular dimensions large enough to require correction. Venus was not a problem because it was so far from Earth at the time that the diameter of the disk was only 0.0027 degree, while the angular beamsize is about 0.009 degree at 32 GHz. A correction factor to account for the partial resolution of the planet's disk by the antenna beam was calculated; the result is 1.03 ± 0.006 (2σ).

Unfortunately, the source structure of Virgo A is neither compact nor very well-known at 32 GHz. Maps of Virgo A have not been published at frequencies above 23 GHz, but relatively good estimates of frequency dependence of the source structure have been made by M. J. Klein. These estimates, derived from maps of the source made at 10 frequencies between 400 MHz and 23,000 MHz, show that the Virgo A size correction for our measurements should be near $C_r = 1.80$. While the structure of the source is known to become more compact at successively higher frequencies, the source structure at 32 GHz is poorly understood. For this reason, we obtained an empirical estimate of C_r by scanning the antenna beam through the source position several times in two orthogonal planes (azimuth and elevation). The procedure was duplicated for the point source 3C273 at very similar azimuth and elevation angles. By comparing the response functions of the scans from the two sources, the value of C_r can be estimated from the apparent beam-broadening produced by the scans across Virgo A, whose angular structure is only slightly smaller than the beam. With the information currently available, the best estimate of the value of C_r is 1.57 ± 0.2 (2σ).

V. Atmospheric Effects

In order to provide antenna characteristics that are independent of the atmospheric attenuation, the atmospheric loss factor needs to be removed from the measurements. One technique (see [3]) to perform this correction uses an efficiency factor given by:

$$L = L_z^{\sec(z)} \tag{19}$$

where L_z is the loss factor (L and $L_z \leq 1$) at the zenith direction, and z is the zenith angle, equal to 90 degrees minus the elevation angle. For these calculations, $L_z = -0.193$ dB $= 0.9565$, which is a typical value for the clear atmosphere present during the observations [3]. To determine the efficiency of the antenna for an ideally transparent atmosphere, the measured efficiency is divided by Eq. (19). This technique is sufficiently accurate for the measurements reported here.

VI. 70-Meter Performance Measurement

A. Observations

After several sessions of calibrations and setup work, the observations were performed on May 3, 4, 6, 8, 11, 15, and July 9, 1989 during both daylight and nighttime conditions. During all but one of these observations, there was exceptionally good weather. The sky was clear for most of the observations, and the effects of the high clouds that occasionally appeared were not detectable in the data. On one date, extremely high winds ($\approx$ 17.8 m/sec) precluded accurate calibrations, but useful information about the performance of the antenna in "near stow" wind conditions was obtained. Given the good observation conditions, there is high confidence in the results described below.

B. Results

1. Aperture efficiency. The efficiency as a function of the elevation angle as directly measured with the radiometer is shown in Fig. 4. This figure shows the discrete data that were measured during the observations for all the sources as well as a second-order fit to the data set. Figure 5 shows the efficiency as a function of elevation for the antenna with the effects of the atmosphere removed. Also shown in this figure is a third-order fit to the data which clearly shows the effects of the exponential secant(z) in the lower elevation angles. The aperture efficiency, as calculated using the curve fit at the reflector set angle of 45 degrees, is found to be 35 percent.

For each data point on the figures, the measurement time is on the order of 8 minutes, which is not optimal for a beam-switching radiometer. This time constraint arose due to a known cyclic oscillation in the hour-angle tracking of the 70-meter antenna that causes the beam to be pointed alternately ahead or behind the source by approx-

imately 0.004 degree, which is approximately equal to the 3 dB beamwidth. This oscillation has a period of 4 minutes; therefore, to perform an observation, one has to chart the data for 4 minutes to select the peak signal, and then run the noise diode calibrator. This operation thus requires 8 minutes. This condition is an example of one use of this radiometer: to determine advisable upgrades for future systems. The problem has been extensively studied by the Ground Antenna and Facilities Engineering Section, and solutions will soon be implemented.

2. Beam shape as a function of elevation. The beam shape of the antenna was measured by performing scans in elevation and cross-elevation. The 3 dB beamwidth at the reflector set angle is 0.009 degree. The beamwidth changes as a function of the antenna elevation angle. Wider beamwidths are seen at the lower and higher elevation angles, whereas the narrowest beamwidths are found near the set elevation angle of 45 degrees. For the data shown in Figs. 4 and 5, source size correction factors are used that are constant as a function of the antenna elevation angle; however, some error is incurred because the antenna beamwidth changes as a function of the angle. This is because the correction factor is related to the antenna beamwidth. Further work must be done to quantify the proper function for the corrections due to finite source sizes; this is another reason to calibrate relative performance using secondary very small, but perhaps variable, sources.

3. Pointing. Focus and pointing of the 70-meter antennas of the DSN are achieved by rotating the subreflector to position the system focus at the feed position on the focal ring. This technique allows a multitude of feeds to be used on the same reflector system. However, the feed system of this radiometer is placed at a position where there is no mechanical pin stop for exact positioning of the subreflector, as there is typically. Analysis showed that the likely error in subreflector positioning due to the lack of this stop would yield a beam direction error of approximately 0.002 degree. This guarantees that the source will always be within the main beam of the antenna. Furthermore, the operational technique for positioning the subreflector includes positioning it to 0 degree, setting the pin that exists for that position, resetting the synchro output, and then moving the subreflector to the 32-GHz feed position. In this way, the subreflector always approaches the desired position from the same direction with the same velocity. For each observation, a pointing exercise is performed that locates the beam bias for the remainder of the observation period. Beam "peaking" is continued during the observation period to assure maximum signal. The pointing model that is used for any feed in the XKR feedcone is accurate enough to ensure that 32-GHz sources always remain within the main beam of the antenna, which is an excellent starting position. Unfortunately, the pointing data that are recorded from observation period to observation period are usually not repeatable.

4. Focus. The focus of the reflector changes as a function of elevation, as it does with pointing. However, the focus change is repeatable from day to day. The focus is defined as the subreflector location along the axis normal to the aperture plane of the reflector that maximizes the RF signal. Figure 6 shows a focus curve of signal versus z-axis position at 27 degrees elevation angle.

C. Comparison to Prediction

The measured value of peak efficiency (35 percent at 45.5 degrees elevation) and the measured efficiency with elevation function were compared to predicted values for the 70-meter antenna. With knowledge of the surface roughness of the 70-meter antenna at Goldstone and a "long-wave" efficiency, i.e., efficiency for a perfectly smooth reflector surface, the 32-GHz performance was predicted.[1] This was done using Ruze's equation for gain degradation due to random surface errors [8]. The expected efficiency at the set angle of 45 degrees elevation was 0.313. The measured value, which was based on assumed flux densities, was 0.35 ± 0.5 (2σ). The difference, 0.04, was less than the uncertainty of the measurements.

VII. Error Sources

The repeatability of the data suggests that the precision of the measurements reported here is very high. The noise diode data are tightly clustered about the mean value; the system response to radio sources varies little from observation to observation on a relative scale; and the system temperature and sensitivity are highly repeatable from day to day. In contrast, the absolute accuracy is much less precise. Several factors that might degrade the accuracy have been identified by category: radio source parameters, noise diode calibration, atmospheric attenuation, and instrumentation.

As discussed above, the flux densities of the radio sources are known with uncertainties of approximately 10 percent (2σ). This source of error might explain why the aperture efficiency values used on Venus are so different from those derived from Virgo A. The peak efficiency (near

[1] D. A. Bathker, "DSS 14 70M Efficiencies Above X-Band Frequencies," JPL Interoffice Memorandum No. 3328-89-0109 (internal document), Jet Propulsion Laboratory, Pasadena, California, May 23, 1989.

45 degrees elevation) from Venus is about 0.38, whereas the corresponding value for Virgo A is only 0.32. The mean of the values is 0.35, which represents our best estimate of the peak efficiency.

It is difficult to determine which source might be more reliable for calibration purposes. The flux density of Virgo A may be incorrect and the correction for source structure (C_r) is poorly known. The flux density spectrum is based primarily on observations below 20 GHz [5]. As measurements at higher frequencies are added, the spectral slope of this multi-component radio source is expected to depart from the linear approximation that is currently in use.

Venus, on the other hand, is expected to exhibit a smoothly variable, featureless spectrum at short centimeter wavelengths [6]. However, the temperature of the Venusian atmosphere, on an absolute scale, is not tightly constrained by models calculated from Earth-based and spacecraft data.

Since neither source is preferable, it was assumed that the mean value is the best estimate of the true efficiency. The Venus data were multiplied by 0.92, and the Virgo A data by 1.08 to remove the adverse effects of the discrepancy on the data plotted in Fig. 5.

Another contributor to error is the noise diode used to set the calibration scale. Errors in the calibration of this noise diode level may be present due to several things: the actual temperature of the cold load is not known (it is assumed to be 77 K); the effect of the liquid nitrogen on the system (reflection, absorption, etc.) may not be negligible at this frequency; ice may have formed in or on the styrofoam tub used to hold the absorber and nitrogen; and there are always errors in the measurement of the various Y-factors [Eqs. (8) through (11)]. The random effect of the atmosphere has been minimized using a beamswitching technique, and the zenith attenuation was assumed, not measured. The system linearity is good but not perfect, and the detectors and power meters also introduce errors.

Finally, the attenuation of the signal due to the axial focus of the subreflector affects the measurements. This effect was investigated during the observations by systematically moving the subreflector in the axial direction (Fig. 6). It was found that the autofocus program that is operating on DSS-14 is near correct, and the signal was frequently maximized in order to minimize this error source.

Tables 5 and 6 list contributors to the calibration errors for the noise diode and system efficiency, respectively. The amount of uncertainty for each contributor is an estimate based on typical measurements of this kind on this present undertaking.

An attempt was made to minimize the error sources over which there was control. Diode calibrations were performed in 5 minutes or less to minimize ice formation problems. Thirty-one diode calibrations were performed using different experimenters to obtain a statistical average of the diode level. This made it possible to quantify random errors. The system was fine-tuned to be as linear as possible. Because of these measures and because observations were performed carefully, it is possible that the absolute error in the efficiency measurements is greater than 10 percent (2σ). Given the excellent agreement between the measured and the predicted values of efficiency for this antenna, it is also possible that sensible estimates of the flux density of the radio sources have been obtained, at least for preliminary performance estimating purposes.

VIII. Concluding Remarks

A series of radiometer calibrations and observations on the 70-meter antenna at Goldstone have been performed in order to characterize its performance at 32 GHz. These observations were done using a beamswitching radiometer with an uncooled HEMT, placed in the XKR feedcone. The calibrations show highly repeatable results indicating a high precision. However, several error sources that will affect the absolute accuracy of the measurements are known. It is calculated that this accuracy is on the order of 10 percent, which in any event is probably less than the absolute accuracy of the natural source flux densities.

In order to perform calibrations of higher accuracy, a program is being developed between Caltech and JPL to perform observations of 100 or more radio sources at the Owens Valley Radio Observatory. The combination of a wideband cooled HEMT amplifier on a high-efficiency (1.5-meter clear aperture) gain standard reflector antenna to measure the very strongest sources and a larger 5-meter antenna to measure numerous weaker sources should allow for significantly increased confidence in natural radio source flux densities at 32 GHz. In particular, the apparent discrepancy between the aperture efficiency values based on Venus measurements and those based on Virgo A will be investigated.

The gain standard reflector has demonstrated good agreement between theoretical and measured estimates and will be very accurately calibrated with National Institute of Standards and Technology traceability. This antenna will be used to accurately calibrate the gain of the 5-meter antenna and thus calibrate the flux density of the 100 or more sources.

Acknowledgments

The authors gratefully appreciate the assistance given by Dave Girdner in solving the many pointing problems associated with the 70-meter antenna at 32 GHz. Thanks also to Dudley Neff for the radiometer packaging and to Carl Ellston and Paul Dendrenos for site support and noise diode calibration.

References

[1] R. H. Dicke, "The Measurement of Thermal Radiation at Microwave Frequencies," *The Review of Scientific Instruments*, vol. 17, pp. 268–275, July 1946.

[2] S. D. Slobin, W. V. T. Rusch, C. T. Stelzried, and T. Sato, "Beam Switching Cassegrain Feed System and its Applications to Microwave and Millimeterwave Radioastronomical Observations," *The Review of Scientific Instruments*, vol. 41, no. 3, pp. 439–443, March 1970.

[3] C. T. Stelzried, "The Deep Space Network—Noise Temperature Concepts, Measurements and Performance," JPL Publication 82-33, Jet Propulsion Laboratory, Pasadena, California, September 15, 1982.

[4] R. M. Dickinson, "A Comparison of 8.415-, 32-, and 565646-GHz Deep Space Telemetry Links," JPL Publication 85-71, Jet Propulsion Laboratory, Pasadena, California, p. 31, October 15, 1985.

[5] J. W. M. Baars, R. Genzel, I. I. K. Pauliny-Toth, and A. Witzel, "The Absolute Spectrum of Cas A: An Accurate Flux Density Scale and a Set of Secondary Calibrators," *Astronomy and Astrophysics*, vol. 61, pp. 99–106, 1977.

[6] P. G. Steffes, M. J. Klein, and J. M. Jenkins, "Observations of the Microwave Emission of Venus from 1.3 to 3.6 cm," *Icarus*, 1989 (in press).

[7] D. O. Muhleman, G. S. Orton, and G. L. Berge, "A Model of the Venus Atmosphere from Radio, Radar, and Occultation Observations," *Astrophysical Journal*, vol. 234, pp. 733-745, 1979.

[8] J. Ruze, "Antenna Tolerance Theory—A Review," *Proc. IEEE*, vol. 54, pp. 633–640, April 1966.

Table 1. System temperature contributions for 32-GHz radiometer[a]

Item	Loss,[b] dB	Temperature, K Contribution	Temperature, K at Reference Plane	Comments
1. Waveguide	−0.75	56.55	56.55	Measured
2. LNA	+50.0	281.5	334.56	Measured
3. T_{atm}	—	—	7.87	Estimated[3]
4. $T_{qs} + T_{so}$	—	—	6.5	Estimated [4]
5. T_{gal}	—	—	3.0	Assumed
6. T_f	—	0.84	1.0	Estimated
7. T_a	—	—	17.37	Lines3 + 4 + 5
8. T_e	—	—	392.11	Lines 1 + 2 + 6
9. T_{op}	—	—	409.48	Lines 7 + 8

[a] Reference plane at the aperture of the feed horn.
[b] Positive value means gain; negative value means attenuation.

Table 2. 32-GHz radiometer operating settings

Item	Setting	Comments
Dicke switching rate	20 Hz	Square-wave rate
Post-detection time constant	1 sec	On lock-in amplifier
Pre-detection time constant	30 msec	On lock-in amplifier
Lock-in amp phase for peak	−23 degrees	On lock-in amplifier
IF bandwidth	32 MHz	IF filter
IF center frequency	64 MHz	IF filter
Level set	10.5 dB	Square-law detector

Table 3. 32-GHz system temperature measurements at DSS-14

Item	Temperature, K	Standard Deviation, K
T_{nd}	10.3	0.2
T_a	16.1	0.5
T_e	399.6	13.5
T_{op}	415.7	13.8

Table 4. 32-GHz calibration sources

IAU Designation	Other names	Measured T_s (el = 45 degrees), K	C_r	Flux density S, Jy[a]		$T_{100\ percent}$, K
				Measured[b]	Assumed	
1228 + 126	Virgo A, 3C274	4.39	1.57	***	14.68	13.03
***	Venus (4 May 89)	14.13	1.03	***	26.70	36.13
***	Venus (8 May 89)	14.48	1.03	***	26.90	36.40
0316 + 412	3C84	21.11	1.00	43.71	***	60.92
1226 − 023	3C273	14.27	1.00	29.54	***	41.17
1328 + 307	3C286	0.98	1.00	1.94	***	2.70
2134 + 004	Parks 2134 + 004	1.87	1.00	3.87	***	5.39

[a] Jy = Jansky = $10^{-26} W m^{-2} Hz^{-1}$
[b] Epoch 1989.4

Table 5. Error contributors to the noise diode calibration (all errors are estimated with confidence of 2σ)

Error Contributor	Error Amount	ΔTnd
ΔTh	±1 K	±0.05 K
ΔTc	±1 K	±0.05 K
$\Delta Y4$	±0.1 percent	±0.45 K
LN2 mismatch	±0.1 percent	±0.45 K
Linearity	±2 percent	±0.05 K
RSS error		±0.64 K

Table 6. Error contributors to efficiency (all errors are estimated with confidence of 2σ)

Error contributor	Error Amount		$\Delta\eta$	
	Venus	Virgo A	Venus, percent	Virgo A, percent
Absolute flux	±11 percent	±12 percent	±4.4	±3.7
C_r	±0.6 percent	±7 percent	±0.2	±2.5
Source Measurement	±0.45 Jy	±0.61 Jy	±0.7	±1.5
T_{nd}	±0.64 K	±0.64 K	±2.0	±2.0
T_{atm}	±2 percent	±2 percent	±1.0	±1.0
Z-focus	±1 inch	±1 inch	±0.8	±0.8
RSS error			±5.05	±5.28

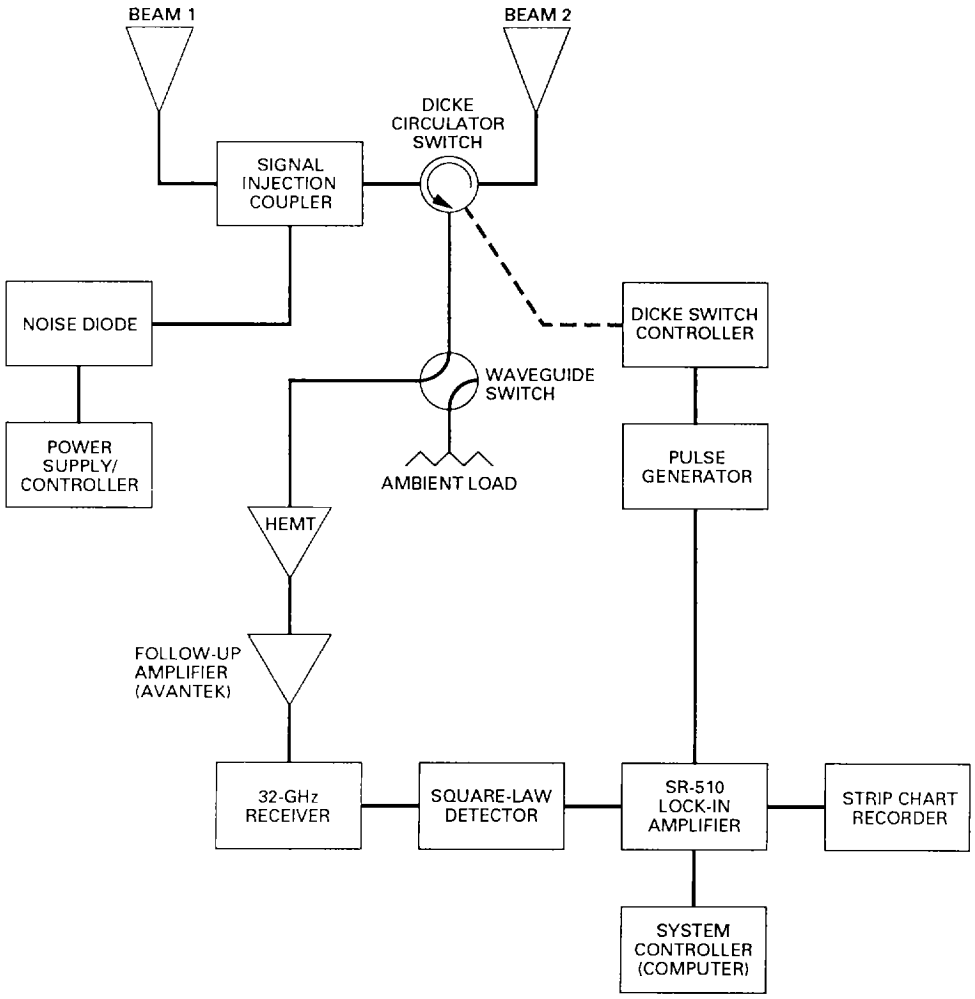

Fig. 1. Block diagram of the 32-GHz beamswitching radiometer.

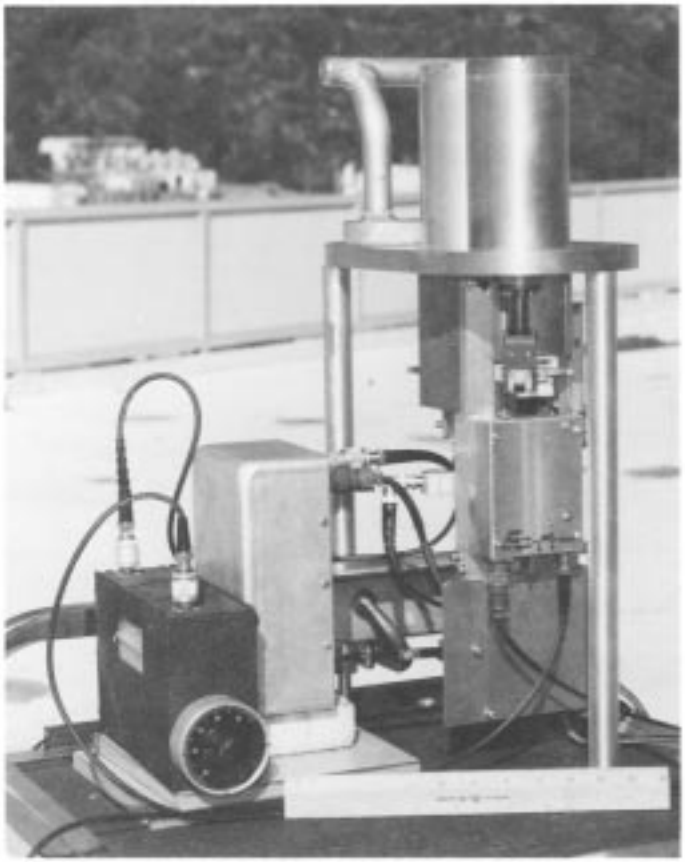

Fig. 2. Dicke radiometer front end.

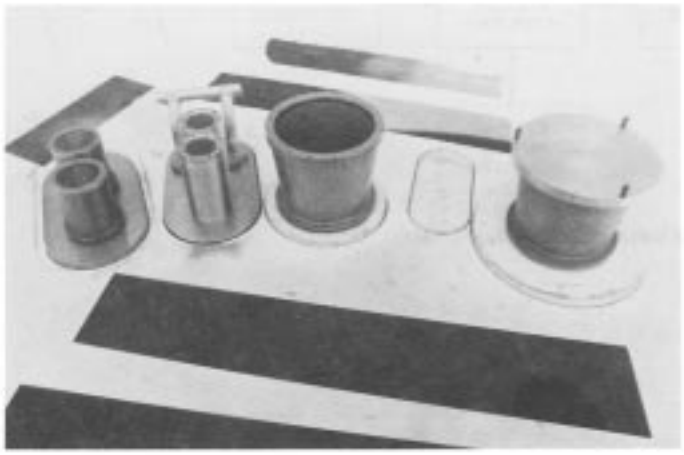

Fig. 3. Top view of XKR feedcone showing various feed systems. (32-GHz radiometer is second from left.)

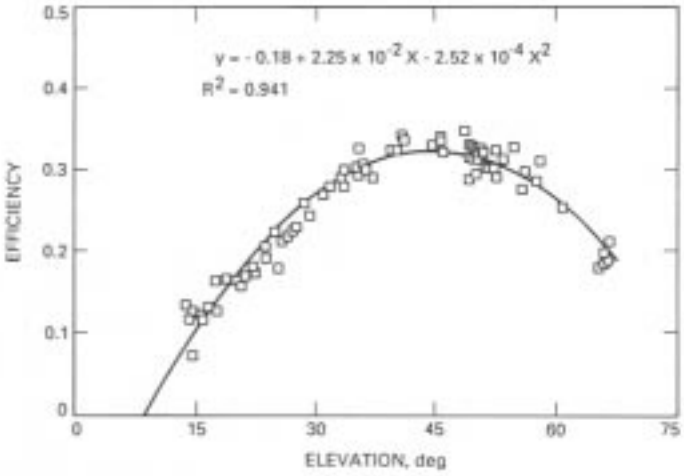

Fig. 4. DSS-14: 32-GHz efficiency including the atmospheric effects (includes second-order fit).

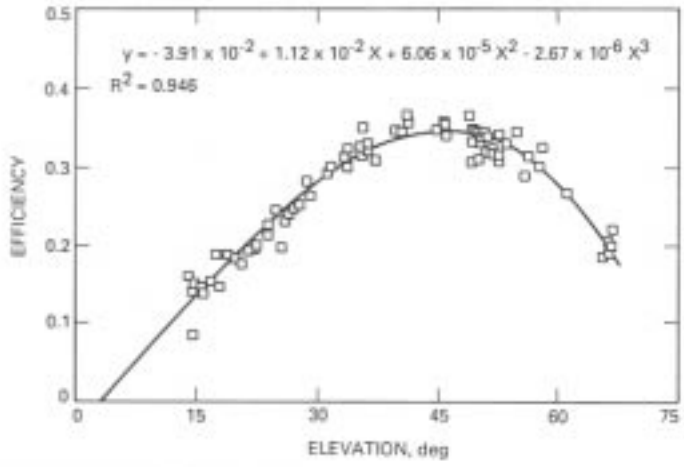

Fig. 5. DSS-14: 32-GHz efficiency; atmospheric effects removed from the data (includes third-order curve fit).

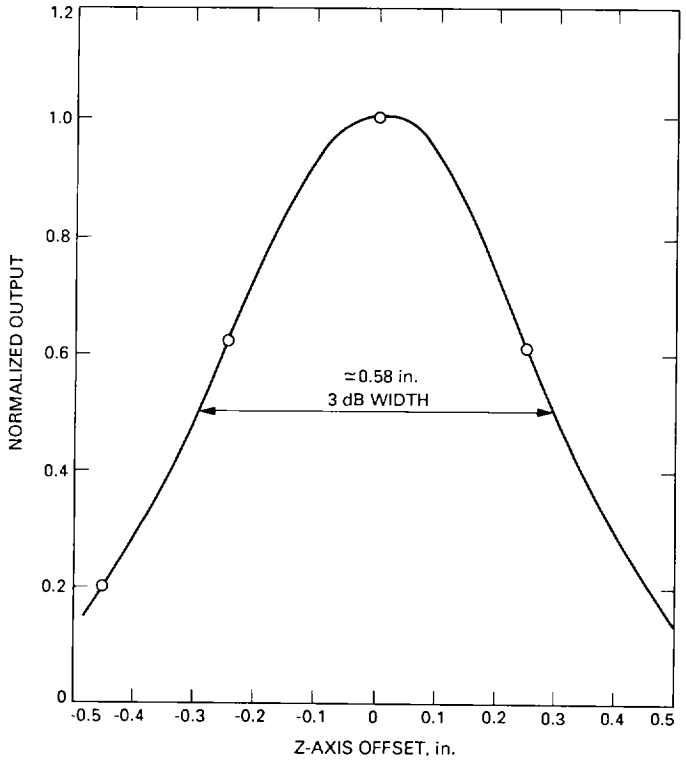

Fig. 6. Z-axis curve. Elevation = 27 degrees. Shows difference from the 70-m standard offset of 2 inches.